ELSEVIER

Discrete Modeling of Short-Fiber Reinforcement in Cementitious Composites

J.E. Bolander Jr.* and S. Saito†
*Department of Civil and Environmental Engineering, University of California, Davis, California; and †Department of Civil Engineering, Kyushu University, Fukuoka, Japan

This article presents a computationally efficient method for analyzing the performance of short-fiber reinforcement in cementitious composites. Each fiber is modeled as a discrete entity. Realistic, nonuniform fiber distributions can be specified as program input. Discrete element systems are used to represent the matrix material. Fiber response is constrained to the kinematics of the discrete elements; the number of system degrees of freedom is therefore independent of the number of fibers. Pre-cracking contributions of the fibers are modeled using an elastic shear lag theory. Post-cracking contributions depend on pullout relations based on the micromechanics of the fiber-matrix interface. In either case, there is a direct link between fiber-local actions and composite response. Numerical results for both aligned and randomly oriented fiber composites are compared with theoretical predictions based on simple mixture rules. ADVANCED CEMENT BASED MATERIALS 1997, 6, 76–86. © *1997 Elsevier Science Ltd.*

KEY WORDS: Cement based materials, Fiber composites, Fiber-matrix micromechanics, Fracture, Random geometry lattice

Effective use of cement based composites depends on controlling the properties of its constituents, which include the matrix material, inclusions such as fibers and aggregates, and the interfacial transition zones (ITZ) between the matrix and inclusions. There is great potential for developing high performance composites using micromechanical models of these basic constituents, as well as other structures that appear at finer scales of observation. The qualifier "high performance" is used to signify cement based materials that meet special requirements [1], which may pertain to: (1) ease of placement and compaction without segregation, (2) long-term mechanical properties, (3) early-age strength, (4) toughness, (5) volume stability, and (6) life in severe environments. Our mostly empirical knowledge of conventional concrete materials does not adequately support the design of such advanced composites. There is a definite need for physically based prediction methods, that is, ones that relate micromechanical models to composite performance in the above categories. For example, prediction of crack width and spacing is important for estimating the durability and service life of structures composed of fiber reinforced cement composites (FRCC). Estimates of strength and ductility are essential for using FRCC in a number of applications, especially where structural components are subjected to shear intensive monotonic and cyclic loadings. Recent research and application development of high performance FRCC has been summarized [2]. Recent developments also include the use of hybrid cement based composites, which are composed of fibers of differing type and functionality [3].

Most analytical models for FRCC are based on single fiber pullout from artificially smooth crack faces. However, the performance of FRCC can neither be predicted nor optimized, solely from information supplied by conventional pullout tests of aligned fibers. There is a need to consider orientation and interaction effects, including how fiber bending interacts with the ITZ and surrounding matrix, loss of efficiency for closely spaced fibers, and microcracking away from the interface. The improved performance associated with higher volume fractions of fibers may be partially, or completely, offset by group interaction effects, higher matrix porosity, and material nonuniformities installed by the production process at higher fiber contents. The effects of nonuniformity of the fiber distributions are not accounted for in most prediction schemes.

Fiber-local micromechanical models are typically related to composite performance through some averaging process or statistical treatment. Such techniques show great potential for engineering application, yet their application to material design is not straightfor-

Address correspondence to: Professor J.E. Bolander Jr., Department of Civil and Environmental Engineering, University of California, Davis, California 95616-5294.
Received December 12, 1996; Accepted April 23, 1997

ISSN 1065-7355/97/$17.00
PII S1065-7355(97)00015-1

ward due to the aforementioned interdependencies between the mechanical parameters and variability in the material distribution. Information is lost during the averaging process, making it more difficult to identify significant mechanisms/interactions and optimize the design accordingly. Likewise, it is difficult to extract such information from experimentation.

This article describes a general approach for modeling short-fiber reinforcement in cementitious composites. Each fiber is modeled as a discrete entity, thus enabling direct relationships between fiber-matrix micromechanics and composite performance. Realistic, nonuniform fiber distributions can be specified as program input. Fibers are constrained to the kinematics of a system of discrete elements composing the matrix. The method is computationally efficient since no additional degrees of freedom are required for modeling the fibers. Fibers may be of any type, although the input parameters for straight fibers of circular cross-section are more closely related to basic constitutive properties. Attention is restricted to so-called macrofibers, whose diameters are large relative to the size of the cement grains and normally range from 0.1 to 1.0 mm.

Pre-cracking contributions of the fibers are modeled using elastic shear lag theory. Fibers that bridge cracks are modeled using line elements with axial and flexural rigidities. Pullout of these elements is based on the micromechanics of the fiber-matrix interface. Some important mechanisms affecting composite performance, such as frictional pulley effects at the exit point of nonaligned fibers, are readily incorporated into the numerical scheme. Other mechanisms related to fiber bending and local bearing of the fiber against the matrix are noted herein and can be addressed by extending this method.

Both aligned fiber and randomly oriented fiber composites are analyzed for direct tensile loadings. Numerical results are compared with theoretical predictions based on ordinary mixture rules. Simple fiber types are considered to enable direct comparisons. The focus is on relating micromechanical models to composite performance, not on the micromechanical models themselves. The numerical and theoretical approaches provide nearly the same results for composite elastic modulus, cracking strength, and the critical volume fraction of fibers defining a transition to multiple cracking. No direct comparisons are made with physical testing of FRCC. As discussed in this article, some further development of the numerical approach is necessary before useful comparisons can be made.

Each numerical test series consists of a number of specimens that differ only in their fiber distributions. Variations in the numerical results, and some systematic differences from the theoretical predictions, are attributed to nonuniformity of these fiber distributions.

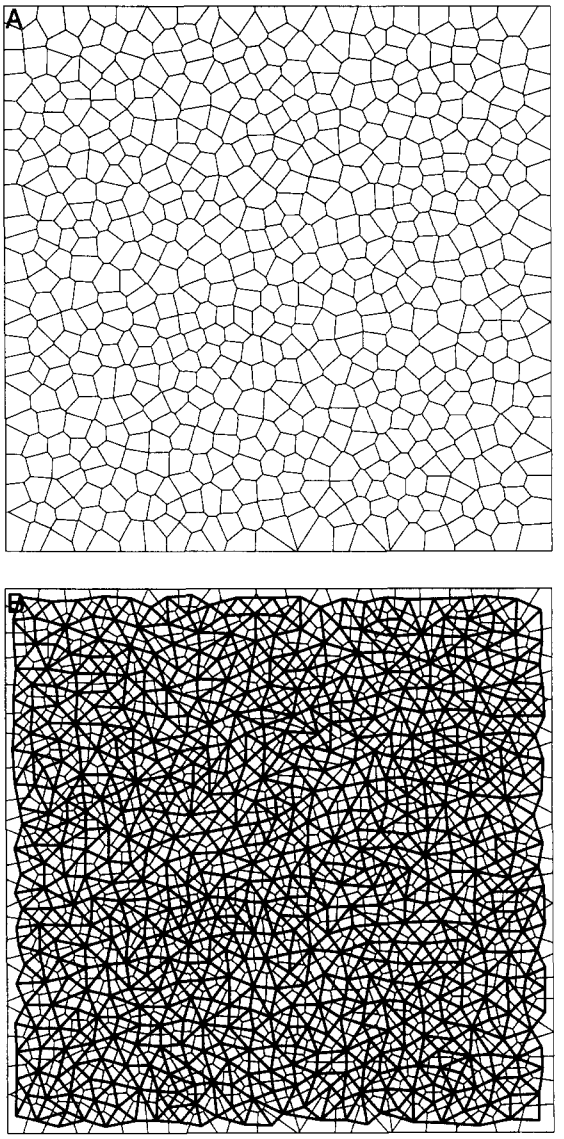

FIGURE 1. Discrete element representation of matrix material: (a) Voronoi polygonal mesh; (b) dual representation—random geometry lattice of beam elements.

The volume fraction of fibers local to first cracking tends to be less than the global volume fraction of fibers. The numerical model readily accounts for other aspects of fiber distribution nonuniformity, including variations in average pullout length and directional bias near the specimen boundaries, which certainly are present in actual materials.

Discrete Element Representation of the Matrix Material

The matrix material is partitioned into a set of convex polygons having random geometry (Figure 1a). Voronoi constructions are used here. Randomness in the mesh

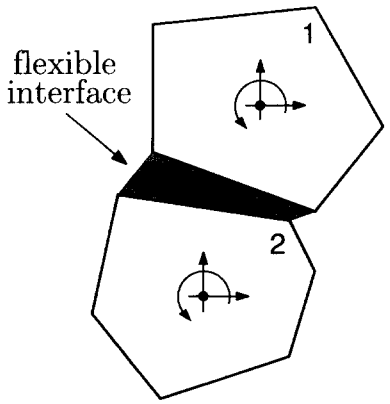

FIGURE 2. Two rigid particles joined by a flexible interface.

design does not represent some local structure of the material, although that is a possibility, but rather is used to minimize bias on cracking direction. Each polygon is regarded as a rigid particle having two translatory and one rotational degree of freedom defined at the particle centroid. Two neighboring particles, displaced under loading and isolated from the mesh, are shown in Figure 2. Particles are interconnected along their edges through flexible interfaces, or equivalently sets of springs, whose stiffnesses are determined to approximate the elastic properties of the overall continuum. A more complete description of this discrete element approach, including formulation of the system equations, is provided by Kawai [4]. Advantages include reduced program complexity (relative to finite element methods), considerable freedom in mesh layout and generation, and a discrete representation of fracture. As will be shown, the approach also provides an efficient means for explicitly modeling short-fiber reinforcement.

The discrete element system is actually a random geometry lattice network of beam elements (Figure 1b). That is, each two-particle assembly acts as a type of beam element connecting the particle centroids. It turns out that beam properties, as determined by the Kawai approach, closely approximate an elastically uniform lattice network. Very little spurious (i.e., nonmaterial related) heterogeneity is introduced prior to cracking, while avoiding the strong anisotropy associated with crack propagation in regular lattices.

Fiber pullout is the dominant toughening mechanism during fracture of FRCC. Representing fiber pullout from the matrix in its multi-cracked limit state is therefore a primary goal of the FRCC modeling strategy. The discrete element system is versatile in representing matrix actions in the post-cracking regime. A coarse mesh of discrete particles has difficulty capturing stress variation near crack tip singularities. However, this is less important when modeling FRCC, since closing pressures exerted by bridging fibers in the crack

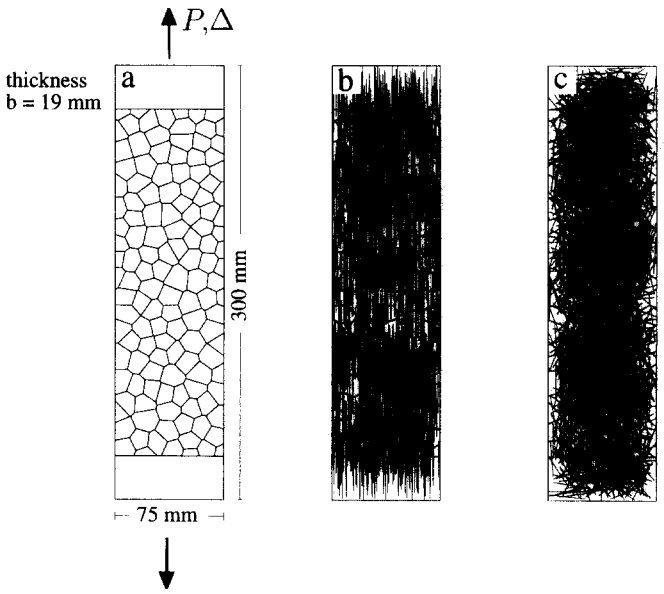

FIGURE 3. Tension specimen modeling: (a) Voronoi discretization of matrix; (b) aligned fiber composite model; (c) random fiber composite model.

wake tend to reduce such singularities. The discrete element model does provide sufficiently accurate stress measures for modifying the fiber pullout relations in response to far-field changes in transverse pressure.

Fracture is represented by degrading the elastic properties of interelemental springs [5]. Fracture energy of the matrix can be realized by progressively softening the elemental interfaces that are experiencing cracking. For tensile loadings, the criterion for fracture is $R = \sigma_n/\sigma_{mu} > 1$, where σ_n is the stress normal to a given interface and σ_{mu} is the unreinforced matrix tensile strength. The interface with the largest $R > 1$ undergoes fracture. Only one fracture is permitted per computational cycle.

Each reinforcing component (e.g., fiber) is projected onto the discrete element discretization of the matrix material. Although the post-cracking actions of the fibers are of primary interest, pre-cracking representation may significantly affect stiffness, cracking strength, and crack development. The pre-cracking and post-cracking actions of the fibers are treated by different modelings, as described in following sections.

Generating Fiber Distributions

Using a pseudo-random number generator, fibers of a prescribed length and diameter are placed in a control volume until a target volume fraction is achieved. Figure 3 shows the projected image of aligned and randomly oriented fiber distributions within models of FRCC tension specimens. Care is taken to keep the fiber

ends within the specimen. This naturally provides directional bias near the specimen boundaries.

The random number generator is not entirely successful in providing isotropic uniformly random fiber distributions away from the boundaries. As will be shown later, nonuniformity significantly affects the computational results. In actual materials, nonuniformity of the fiber distribution arises from the presence of aggregate inclusions, gravitational effects, proximity to specimen boundaries, and methods of dispersion and mixing during the production process. Fiber distributions have been studied experimentally [6] and can be determined using stereological image analyses techniques [7]. Realistic distributions of inclusions, both fiber and aggregate, can be simulated through dynamical mixing processes, which account for the forces acting on the particles during production [8]. Rather than the simplistic methods used in this article, such techniques could be used for simulation of the fiber and aggregate distributions in actual materials.

Pre-Cracking Representation of Fibers

Prior to cracking, fiber stiffness contributions are based on the mechanics of elastic stress transfer between the fiber and surrounding matrix. Details of the pre-cracking representation of fibers have been reported previously [9]. An overview of the procedure is provided here.

Fiber local stiffness is determined using any appropriate model that relates fiber axial stress to matrix strain. The following relation, provided by Cox [10], is used here:

$$\sigma_f(x) = E_f \epsilon_m \left[1 - \frac{\cosh\left(\beta_1 \left(\frac{\ell}{2} - x \right) \right)}{\cosh(\beta_1 \ell / 2)} \right] \quad (1)$$

where x is the distance from either fiber end, E_f is the fiber modulus of elasticity, ϵ_m is the strain in the matrix in the fiber direction, and ℓ is the fiber length. Parameter β_1 is defined as:

$$\beta_1 = \left[\frac{2G_m}{E_f r^2 \ln(R/r)} \right]^{1/2} \quad (2)$$

where R is the effective radius of the matrix around the fiber, r is the fiber radius, and G_m is the matrix shear modulus at the interface. The ratio R/r depends on fiber arrangement and fiber volume fraction, V_f [11]. No relative displacement occurs at the fiber-matrix interface. Furthermore, there are no interactions between the stress fields arising from different fibers. Additional assumptions supporting eq 1 have been listed elsewhere [11].

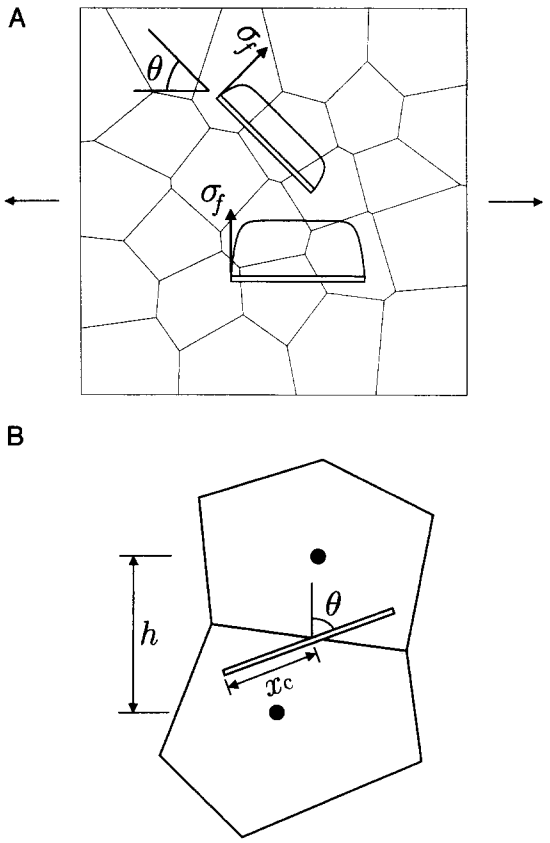

FIGURE 4. Fiber representation before cracking: (A) fibers in matrix under uniaxial tension; (B) single fiber crossing an elemental boundary.

Figure 4a shows stress distributions provided by eq 1 for fibers of differing orientation, θ, with respect to the loading direction. Axial stress in a fiber decreases with increasing θ. The stress in the fiber at an elemental boundary crossing is used to define the fiber stiffness contribution to the local two-particle assembly (Figure 4b). Fiber axial stiffness local to the crossing can be approximated by [9]:

$$k_f = A_f E_f \frac{\cos\theta}{h} \left[1 - \frac{\cosh\left(\beta_1 \left(\frac{\ell}{2} - x_c \right) \right)}{\cosh(\beta_1 \ell / 2)} \right] \quad (3)$$

where A_f is fiber cross-sectional area, x_c is the distance from the end of the fiber to the crossing, and h is the distance between neighboring particle centroids in the direction of loading. This quantity transforms into global stiffness measures defined at the particle centroids [9].

An estimate of the composite elastic modulus is used here to verify the numerical procedure. According to the rule of mixtures:

Adv Cem Bas Mat
1997;6:76–86

TABLE 1. Composite modulus predictions (aligned fibers)

V_f (%)	ℓ/d	$\overline{\hat{E}_c/E_c}$	$\bar{\gamma}$	σ_γ
1.0	100	1.00024	0.00043	0.00322
1.0	60	0.99966	−0.00635	0.00648
2.0	100	0.99996	−0.00043	0.00539
2.0	60	0.99970	−0.00292	0.00612
4.0	100	1.00007	0.00036	0.00182
4.0	60	0.99902	−0.00529	0.00291

$$E_c = (1 - V_f) E_m + \eta_\ell \eta_\theta V_f E_f \tag{4}$$

where η_ℓ and η_θ are factors expressing the length and orientation efficiency of short fibers relative to long aligned fibers prior to cracking [11]. Parameters η_ℓ and η_θ are defined so as to parallel the assumptions made in the numerical modeling. Letting $\eta_\ell = \bar{\sigma}_f/(E_f \epsilon_m)$, where $\bar{\sigma}_f$ is the average axial stress in the fiber as given previously [11], yields:

$$\eta_\ell = 1 - \frac{\tanh(\beta_1 \ell/2)}{\beta_1 \ell/2}. \tag{5}$$

For uniaxial loading of a two-dimensional model, as shown in Figure 4a, a measure of stiffening efficiency of randomly oriented fibers prior to cracking is:

$$\eta_\theta = \frac{1}{N} \sum_{i=1}^{N} \cos^4 \theta_i \tag{6}$$

where N is the total number of fibers.

The numerical composite modulus, $\hat{E}_c$, is determined by imposing an axial deformation on a numerical specimen, examples of which are shown in Figure 3, and then measuring the reactive force. Comparisons between $\hat{E}_c$ and E_c are made for two different fiber aspect ratios of both aligned and randomly oriented short fibers. $\eta_\theta = 1$ for fibers aligned with the loading direction. $\eta_\theta = 0.375$ for an isotropic uniformly random distribution of fibers. Due to directional bias near the specimen boundaries, however, $\eta_\theta = 0.427$ for the distribution shown in Figure 3c.

Tables 1 and 2 compare the numerical and theoretical predictions of composite modulus for aligned and randomly oriented fibers, respectively. Overbars indicate average values from five numerical tests. At very low fiber contents the composite modulus approaches that of the matrix; therefore, $\gamma = (\hat{E}_c - E_c)/(\hat{E}_c - E_m)$ is given for comparison. σ_γ is the standard deviation of this value. Mean values for composite modulus are within ±0.2% of the theoretical predictions; most values are well within this range. Such accuracy is remarkable considering some of the specimens (i.e., those with V_f = 4% and ℓ/d = 100) contain over 12,000 individual fibers. Although these results are based on different random fiber distributions, there is little variation in the composite moduli within each series of numerical tests. Objectivity of the pre-cracking FRCC model has been studied through numerical testing. The results indicate the contribution of fibers to composite modulus is virtually independent of random mesh design and the degree of mesh refinement within certain limits. For example, element densities twice as great as that shown in Figure 3 provide nearly the same results as those given in Tables 1 and 2. Further study is needed to determine if objectivity is maintained in the limit sense, that is, as the mean element size approaches the diameter of the fiber.

TABLE 2. Composite modulus predictions (randomly oriented fibers)

V_f (%)	ℓ/d	$\overline{\hat{E}_c/E_c}$	$\bar{\gamma}$	σ_γ
1.0	100	1.00068	0.03494	0.00684
1.0	60	1.00053	0.02812	0.02210
2.0	100	1.00125	0.03282	0.00461
2.0	60	1.00098	0.02687	0.00880
4.0	100	1.00190	0.02575	0.00867
4.0	60	1.00170	0.02401	0.00694

Equation 1 is derived for a two-phase elastic composite. Alwan and Naaman [12] introduced a third phase, i.e., a zero volume interfacial layer surrounding the fiber, to better model stress transfer between the matrix and fiber. The interfacial layer may have mechanical properties differing from those of the bulk matrix. Such an approach can be accommodated within our analysis framework simply by replacing eq 1 with an appropriate stress transfer relation. Najm and Naaman [13] adjust the matrix elastic modulus to account for porosity as affected by the presence of fibers. Similar steps can be taken here.

Fiber Pullout

During cracking, regular beam elements are inserted to represent fibers bridging opposing crack faces. Constraint equations relate beam nodal displacements to those at the discrete element centroids. The treatment of axial and flexural actions is uncoupled: a micromechanical model is used to describe the nonlinear process of fiber debonding and pullout; fiber flexural response is linear elastic. No debonding is allowed prior to matrix cracking, as might occur at the fiber extremities if the matrix strength is high. Interaction effects between fibers bridging a crack are not considered here, although this could be done in an approximate, phenomenological way by modifying a fiber's pullout response according to the proximity, orientation, and actions of neighboring fibers. The development of mi-

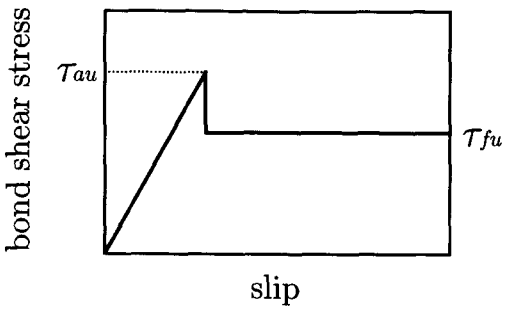

FIGURE 5. Bond stress-slip relation.

cromechanically based interaction models requires better local descriptions of matrix strain and damage than are supplied by the current approach.

Either a mechanics of composite materials approach or a fracture mechanics approach can be used to model the debonding process along the fiber-matrix interface [14]. The former approach is used here to determine the load-pullout relation for each embedded length [15,16]. Naaman et al. [16] account for such factors as adhesional and frictional strengths along the interface, matrix-fiber misfit, modular ratio between matrix and fiber, and degradation of frictional strength during the advanced stages of loading. Using equilibrium and compatibility conditions, a composite pullout curve is derived from the pullout relation for each embedded length [17]. With continued opening, the shorter embedded length eventually pulls out, while the longer length unloads after peak load. In essence, the micromechanical relations between the fiber and matrix are lumped into a nonlinear spring acting across the crack face. Fiber rupture occurs if the stress in the fiber exceeds a preset value, f_r. Unloading/reloading follows a multiple of the secant branch defined by the current point on the pullout curve. For the results that immediately follow, the pullout relation is assumed to be independent of entry angle, as if a frictionless pulley redirects fiber axial force about the exit point.

Figure 5 shows the bond stress-slip relation utilized for straight nondeformed fibers. τ_{au} and τ_{fu} are the adhesional and frictional shear bond strengths of the fiber-matrix interface. τ_{fu} can be modified to account for slip-weakening or slip-hardening of the interface. Such bond stress-slip relations are constitutive properties of the interface and therefore preferable as program input. For deformed shape fibers, bonding is primarily due to mechanical actions that cannot be modeled correctly in terms of interfacial shear stresses during pullout. If the pullout curve is available, however, the analysis can still be performed. From the pullout curve, it is straightforward to include the contribution of the fiber to both the system stiffness matrix and the out-of-balance force vector during conventional nonlinear analyses [9].

Prior to cracking, a fiber crossing over several particles contributes stiffness to each of the particle subassemblies, as previously described. During cracking, however, some simplification is necessary to avoid modeling pullout at multiple locations along a single fiber. At this stage of program development, the first subassembly to experience fracture is used to define subsequent fiber response, i.e., define the pullout location and thus the fiber embedded lengths. The fiber continues to contribute elastic stiffness to the other associated subassemblies unless cracking occurs there, too. This places some restrictions on the relative sizes of the particles and fiber lengths. If a large percentage of the fibers cross more than one particle boundary, there may be difficulties in modeling distributed fracture.

The specimens shown in Figure 3 are subjected to displacement controlled tensile loading. Smooth, straight, randomly oriented fibers that have high modulus and high strength are used. $V_f = 0.75\%$, $\ell/d = 100$, $\tau = \tau_{au} = \tau_{fu}$, and $\tau/\sigma_{mu} = 1$. Fiber force-pullout relations are patterned after those presented by Naaman et al. [16]. Any effects due to bearing of the fibers against the matrix at the fiber exit point are neglected. The load-deformation response shown in Figure 6a indicates a sudden decrease in reactive force following matrix fracture. The relatively low volume fraction of fibers does not provide sufficient load transfer to cause further cracking. Localization of damage at first cracking leads to failure (Figure 6b). Although this specimen exhibits composite strain much higher than the failure strain of the unreinforced matrix, the benefits achieved may not be enough to warrant fiber additions in many applications. More effective material designs can be realized if multiple cracking occurs, as described next.

Multiple Fracture

Multiple cracking will occur if the post-cracking strength of the composite is greater than the first cracking strength [18]:

$$\sigma_{pc} \geq \sigma_{cc}. \tag{7}$$

Cracking strength of the composite can be estimated using:

$$\sigma_{cc} = \sigma_{mu}(1 - V_f) + \alpha_1\alpha_2\tau V_f\frac{\ell}{d} \tag{8}$$

where σ_{mu} is the direct tensile strength of the unreinforced matrix, τ is the average bond strength at the fiber-matrix interface, α_1 is the fraction of bond strength acting at first matrix cracking, and α_2 is a factor accounting for the orientation efficiency of the fibers prior to cracking.

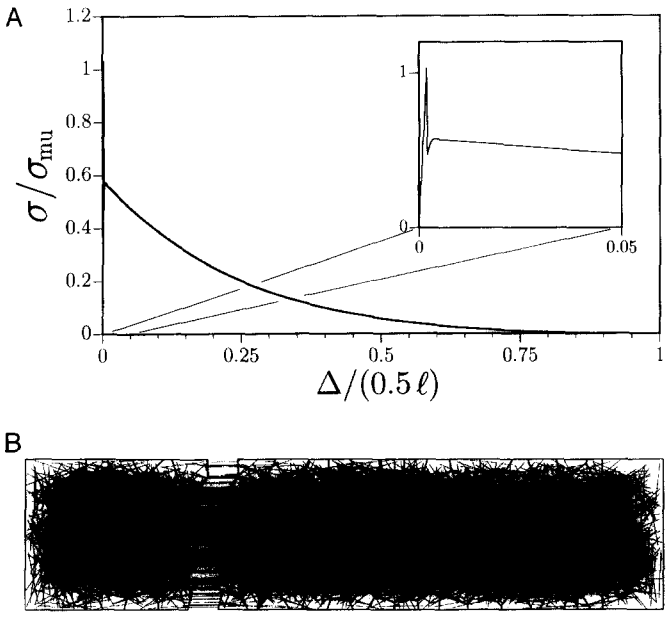

FIGURE 6. Tension specimen exhibiting localized fracture: (A) load-displacement diagram; (B) deformed mesh.

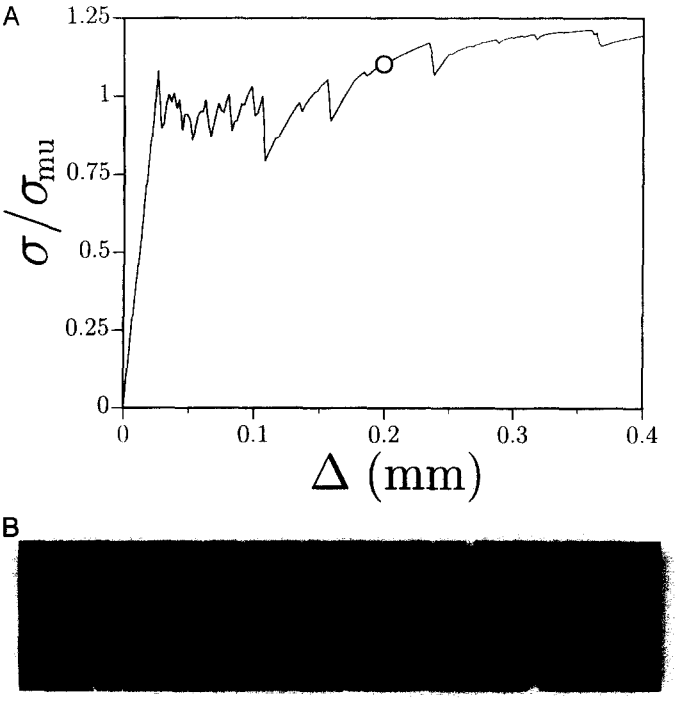

FIGURE 7. Tension specimen exhibiting distributed fracture: (A) load-displacement diagram; (B) deformed mesh.

Assuming an average pullout length of $\ell/4$ and no interaction effects between neighboring fibers, post-cracking strength of the composite is given by:

$$\sigma_{pc} = \lambda \tau V_f \frac{\ell}{d} \tag{9}$$

where λ is a factor accounting for a number of effects, including orientation efficiency of the fibers after cracking, possible plastic yielding of the fiber near the exit points, and increased frictional resistance, crushing, and/or spalling due to fiber bearing against the ITZ and matrix near the exit points.

Increasing the volume fraction of fibers induces a type of multiple cracking indicative of high performance FRCC. For example, the previous fracture analysis (Figure 6) is performed after increasing the volume fraction of fibers to $V_f = 2\%$ and including frictional pulley effects at the fiber exit points (as described later.) Figure 7 shows damage distributed throughout the mesh as the specimen approaches peak load, as indicated on the accompanying stress-displacement curve. The limited strain capacity realized here is due to the type of fibers selected. Prior to quasi-strain hardening, multiple cracking initially proceeds at section average stresses less than the first cracking stress, that is, $\sigma \leq \sigma_{cc}$. Both fiber distribution nonuniformity and the lumping of pullout force at the fiber exit point tend to cause small pieces of the matrix (i.e., one or more discrete elements) to break off locally. Fiber forces need be distributed along the embedded length and lumped appropriately at all crossing points. Such an approach is necessary for preventing spurious breakoff of smaller particles and producing mesh-independent crack spacings.

The critical volume fraction of fibers, $(V_f)_{cr}$, defines the transition from single cracking with localized failure to multiple cracking with possible quasi-strain hardening. An estimate of $(V_f)_{cr}$ can be obtained by equating σ_{pc} and σ_{cc}, as expressed by eqs 8 and 9 [18]. This estimate assumes fracture occurs simultaneously through the specimen width. Note in the previous result there is a tendency for one-sided crack growth, which may not completely traverse the cross-section before secondary crack formation. For comparing with theory we use a simpler mesh of rectangular elements to represent the composite as shown in Figure 8a. Fracture then occurs through the entire cross-section simultaneously.

The numerical prediction of $(V_f)_{cr}$ is performed by adjusting the global number of fibers until the conditions for multiple cracking expressed by eq 7 are just met. For example, Figure 8b shows the composite pullout curve for a specimen with V_f just less than the critical value. Figure 9 compares the numerical $(V_f)_{cr}$ obtained in this manner with theoretical values given by eqs 7–9. Each data point for the numerical analyses is the mean value from seven numerical tests; the bars indicate 1 SD about the mean value. Increasing bond strength clearly improves the efficiency of fibers, provided fiber rupture does not occur.

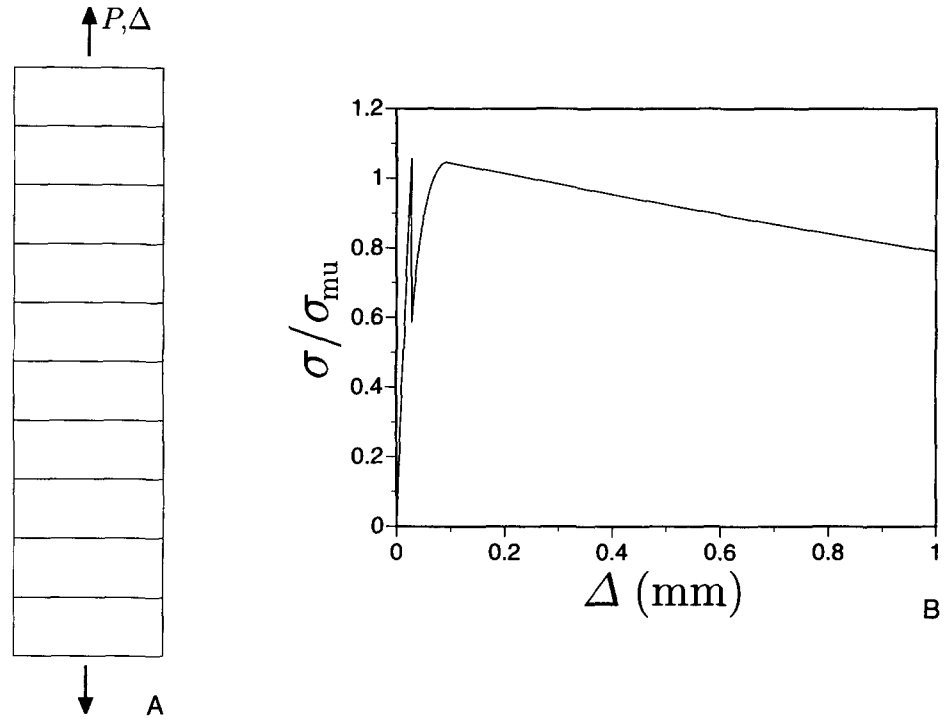

FIGURE 8. Tension specimen modeling: (A) rectangular mesh; (B) load-displacement diagram.

Parameter α_1 in eq 8 is determined from the axial stress in each fiber at cracking, as provided by the numerical model. α_2 is the average value of $\cos^2 \theta_i$, as computed from all fibers ($i = 1 \ldots N$) in the distribution. Cracking strengths given by eq 8 agree with those from the numerical model. Parameter λ is set equal to the average value of $\cos \theta_i$. Only the geometrical effects of fiber orientation are accounted for in these numerical and theoretical predictions of critical volume fraction. Frictional effects at the fiber exit point are considered in a later section.

Slightly higher critical volume fractions are predicted by the numerical model in nearly all cases. Due to nonuniformity of the fiber distributions used for the numerical analyses, the section with the least stiffness contribution from the fibers is the first location to experience fracture. The V_f local to the first fracture, computed from the number of fibers crossing the fracture plane, may be significantly less than the target V_f provided by the fiber generation program (Figure 10). Crack locations are restricted by the coarseness of the matrix mesh; therefore, even weaker zones may exist within the composite material. There is also variation in the average pullout length of fibers bridging the first fracture plane, as shown in Figure 11. The mean average pullout length is close to its expected length, $\ell/4$. Differences in average pullout length, at the first and subsequent fractures, greatly affect $(V_f)_{cr}$ given by the numerical model.

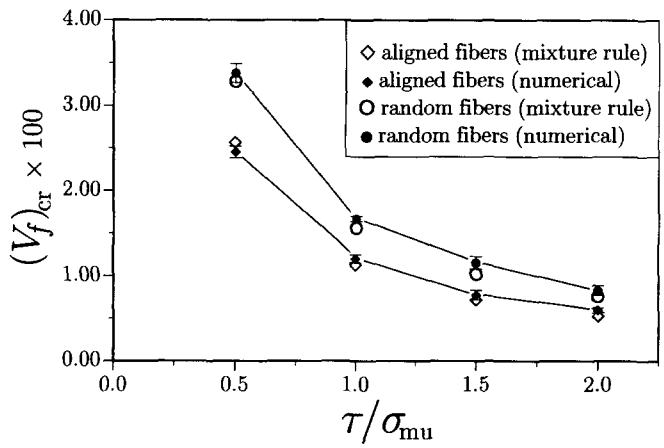

FIGURE 9. Predicted critical volume fractions.

The numerical $(V_f)_{cr}$ values given here only ensure that more than one crack forms; they are therefore lower bound estimates of the $(V_f)_{cr}$ needed for the extensive multiple fracture indicative of high performance FRCC. Higher global volume fractions are needed to offset the relative weakness of the first fractures resulting from nonuniform fiber distributions. Continued multiple cracking can only proceed along with some degree of strain hardening of the composite. Quasi-strain hardening has been attributed to the nonuniform distribution of flaw sizes in the matrix [19]. The results given here also point to influences from variabil-

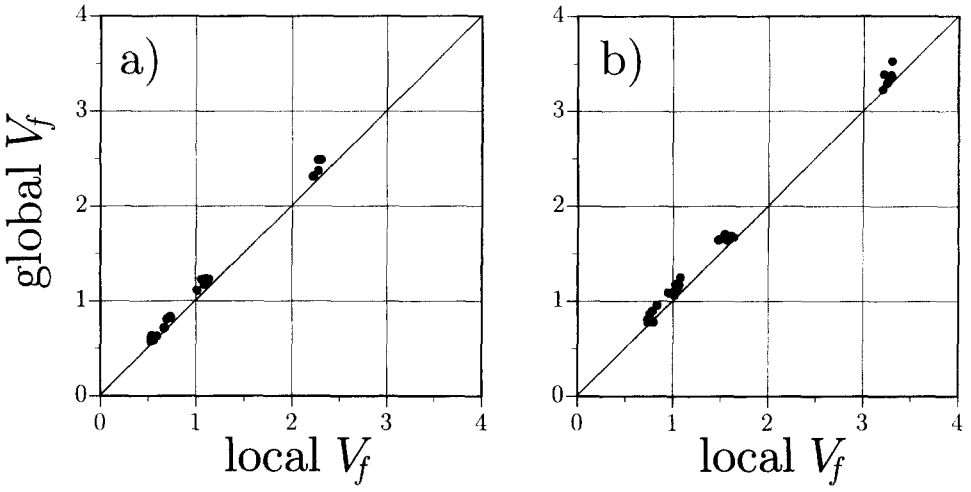

FIGURE 10. Local volume fraction of fibers at first crack section: (a) aligned fibers; (b) randomly oriented fibers.

ity in the fiber distribution. The differences seen here are significant even though the fiber generation routine aimed to produce a uniformly random distribution. Provided accurate methods for defining the fiber distributions are available, the numerical model given here can be used to analyze actual materials where variability is likely to be greater.

Quantitative comparisons with experimental results will help guide future development of this numerical approach. The ordinary mixture rules, as used here for comparison, may overestimate fiber reinforcing efficiency as they have not been adjusted to reflect fiber group interaction effects and damage processes active at the fiber exit point, including matrix spalling. Furthermore, cracks propagating through the composite can produce microcracking along the interface and within the ITZ [11], possibly reducing fiber efficiency. The analyses performed here are two-dimensional, whereas a third dimensional component is present in most tests, again reducing fiber reinforcing efficiency.

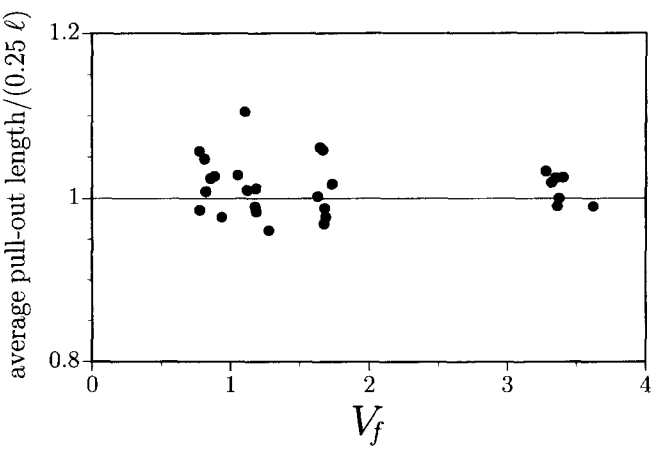

FIGURE 11. Variation in average pullout length at first fracture (randomly oriented fibers).

Frictional Resistance at Fiber Exit Point

Certain types of ductile low modulus fibers, which are inclined to the loading direction, may show increased pullout resistance due to frictional stresses acting near the fiber exit point [20,21]. This friction is caused by fibers bearing against the matrix while undergoing local bending. The resistance increases with increasing inclination angle up to a certain limit after which the matrix becomes prone to spalling. Through both experimental and theoretical work, Ouyang et al. [20] developed a relation for the pullout force of such inclined fibers:

$$P_\theta = \frac{1}{\cos\theta} P \tag{10}$$

where θ is the inclination angle and P is the pullout force associated with fibers aligned in the loading direction. It was observed that this relation holds for $-45 \leq \theta \leq 45°$. An exponential equation expressing similar relationships is given by Li et al. [21].

The previous numerical results for $(V_f)_{cr}$ for randomly oriented fibers are now compared to those modified for frictional pulley effect according to eq 10. In the absence of matrix spalling or fiber rupture, the increased frictional resistance at the fiber exit point increases the efficiency of the reinforcing to nearly that of aligned fibers (Figure 12).

Conclusions

This article introduces a computationally efficient method for analyzing the performance of short-fiber reinforce-

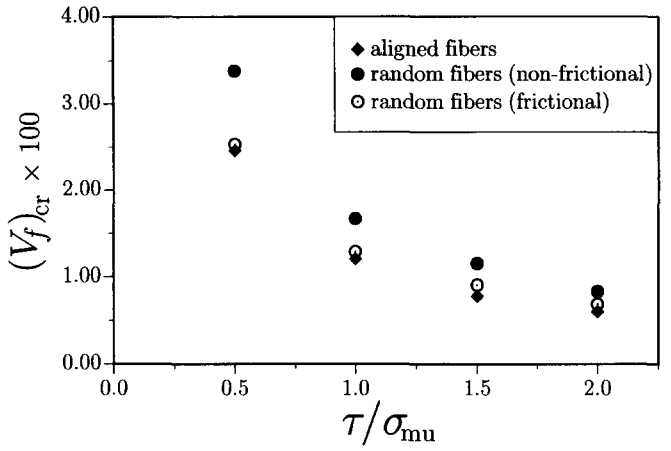

FIGURE 12. Increased efficiency of inclined fibers due to frictional pulley effect.

ment in cementitious composites. Each fiber in the composite is treated as a discrete entity. Fiber actions are constrained to the kinematics of a discrete element system representing the matrix material; the number of system degrees of freedom is therefore independent of the number of fibers. Both prior to and after cracking, there is a direct link between fiber-local actions and composite response. This new approach offers a level of control and inspection that is not attainable using fiber models based on average quantities defined over a representative material volume.

The pre-cracking representation of fiber stiffness is quite general in that it only requires a relation expressing axial stress in the fiber as a function of matrix strain. Although a two-phase elastic composite model was used here, application of a three-phase composite model, such as that described by Alwan and Naaman [12], would be straightforward.

Numerical results for both aligned and randomly oriented fiber composites are compared with theoretical predictions based on simple mixture rules. Several numerical specimens, differing only in fiber distribution, are tested for each parameter setting. The efficiency parameters in the mixture rules were based on the assumed fiber distributions. The numerical specimens provided mean values for composite modulus that are within ±0.2% of the theoretical predictions. Most values are well within this range.

The numerical approach simulates a transition from single to multiple cracking with increasing volume fraction of fibers. Nonuniform crack growth occurs when using random geometry elements; this complicates comparisons with mixture rules that assume simultaneous fracture over the cross-section. Using simpler rectangular elements, the numerical approach and the mixture rules predict nearly the same the critical volume fraction of fibers, $(V_f)_{cr}$. Variation in the numerical results, and the tendency for the numerical model to predict higher $(V_f)_{cr}$, is due to nonuniformity of the fiber distributions. The volume fraction of fibers local to first cracking is less than the global volume fraction. Higher fiber contents are necessary to compensate for this effect when designing for multiple cracking. These effects are evident even for the seemingly uniform distributions generated with a pseudo-random number generator. Other features of actual materials, such as variations in average pullout length and directional bias of the fibers near the specimen boundaries, are realized by the numerical approach. Discrete modeling of each fiber provides a direct means for studying the effects of fiber distribution nonuniformity on the composite performance.

To enable direct comparisons with theoretical results, the numerical analyses focused on simple fibers under rather ideal conditions. The numerical approach needs further development for investigating the behavior of more realistic materials. Model objectivity with respect to element size and mesh geometry is another area that needs careful study, particularly when analyzing distributed cracking. Nonetheless, the close agreement between numerical and theoretical results presented here is remarkable, considering the qualities of the matrix material model and that thousands of fibers are being modeled in a discrete manner. With further development, this discrete modeling of short-fiber reinforcement has the potential to resolve basic parameter interdependencies, foster the development of macromodels for larger scale engineering analyses, and support the optimization of FRCC materials.

References

1. *High-Performance Construction Materials and Systems.* Technical Report 93-5011 prepared by the Civil Engineering Research Foundation (CERF) and the Planning Committee for the Nationally-Coordinated Program on High-Performance Concrete and Steel, April 1993.
2. Naaman, A.E.; Reinhardt, H.W.; Eds. *High Performance Fiber Reinforced Cement Composites 2 (HPFRCC 2).* E & FN SPON: London, 1996.
3. Mobasher, B.; Li, C.-Y. *ACI Mater. J.* **1996,** *93,* 284–292.
4. Kawai, T. *Nucl. Eng. Design* **1978,** *48,* 207–229.
5. Liu, Y.-Q.; Hikosaka, H.; Bolander, J.E. In *Fracture Mechanics of Concrete Structures;* Wittmann, F.H., Ed.; Aedificatio Publishers: Freiburg, Germany, 1995; pp. 375–382.
6. Stroeven, P.; Shah, S.P. In *Testing and Test Methods for Fibre Cement Composites;* Swamy, R.N., Ed.; The Construction Press: UK, 1978; 275–288.
7. Stroeven, P. In *Advanced Technology for Design and Fabrication of Composite Materials and Structures;* Sih, G.C.; Carpinteri, A.; Surace, G., Eds.; Kluwer Academic Publishers: Norwell, MA, 1995; pp. 203–219.
8. Stroeven, P.; Stroeven, M. In *New Developments in Concrete*

Science And Technology; Nanjing, China, 1995.
9. Bolander, J.E. University of California, Davis, Department of Civil & Environmental Engineering Report, 1996.
10. Cox, H.L. *Br. J. Appl. Phys.* **1952,** *3*, 72–79.
11. Bentur, A.; Mindess, S. *Fibre Reinforced Cementitious Composites*; Elsevier Science Publishers Ltd.: London, 1990.
12. Alwan, J.M.; Naaman, A.E. *ASCE J. Eng. Mech.* **1994,** *120*, 2443–2461.
13. Najm, H.; Naaman, A.E. *ACI Mater. J.* **1994,** *91*, 122–130.
14. Stang, H.; Li, Z.; Shah, S.P. *ASCE J. Eng. Mech.* **1990,** *116*, 2136–2150.
15. Gopalaratnam, V.S.; Shah, S.P. *ASCE J. Eng. Mech.* **1987,** *113*, 635–652.
16. Naaman, A.E.; Namur, G.; Alwan, J.M.; Najm, H. *ASCE J. Eng. Mech.* **1991,** *117*, 2769–2790.
17. Li, V.C.; Wang, Y.; Backer, S. *J. Mech. Phys. Solids* **1991,** *39*, 607–625.
18. Naaman, A.E.; Reinhardt, H.W. In *High Performance Fiber Reinforced Cement Composites 2 (HPFRCC 2)*; Naaman, A.E.; Reinhardt, H.W., Eds.; E & FN SPON: London, 1996, pp. 1–24.
19. Wu, H.C.; Li, V.C. *Int. J. Damage Mech.* **1995,** *4*, 83–102.
20. Ouyang, C.; Pacios, A.; Shah, S.P. *J. Eng. Mech.* **1994,** *120*, 2641–2659.
21. Li, V.C.; Wang, Y.; Backer, S. *Composites* **1990,** *21*, 132–140.